

## Gold Nanoparticles: Past, Present, and Future<sup>†</sup>

Rajesh Sardar,<sup>‡</sup> Alison M. Funston,<sup>§</sup> Paul Mulvaney,<sup>\*,§</sup> and Royce W. Murray<sup>\*,‡</sup>

<sup>‡</sup>*Kenan Laboratories of Chemistry, University of North Carolina, Chapel Hill, North Carolina 27599, and*

<sup>§</sup>*School of Chemistry and Bio21 Institute, University of Melbourne, Parkville, Victoria, 3010, Australia*

*Received June 1, 2009. Revised Manuscript Received June 12, 2009*

This perspective reviews recent developments in the synthesis, electrochemistry, and optical properties of gold nanoparticles, with emphasis on papers initiating the developments and with an eye to their consequences. Key aspects of Au nanoparticle synthesis have included the two-phase synthesis of thiolated nanoparticles, the sequestration and reduction of Au salts within dendrimers, the controlled growth of larger particles of well-defined shapes via the seeded approach, and the assembling of a variety of nanoparticle networks and nanostructures. The electrochemistry of thiolated Au nanoparticles is systemized as regions of bulk-continuum voltammetry, voltammetry reflective of quantized double-layer charging, and molecule-like voltammetry reflective of molecular energy gaps. These features are principally determined by the nanoparticle core. Interesting multielectron Au nanoparticle voltammetry is observed when the thiolate ligand shell has been decorated with redox groupings. Another development is that Au nanoparticles were discovered to exhibit unanticipated properties as heterogeneous catalysts, starting with the low-temperature oxidation of CO. Substantial progress has also been made in understanding the surface plasmon spectroscopy of Au nanoparticles and nanorods. The need to investigate the optical properties of metal particles of a single, well-defined shape and size has motivated the development of a number of new techniques, leading to the study of electron transfer and redox catalysis on single nanoparticles.

### Introduction

Gold nanoparticle chemistry and physics has emerged as a broad new subdiscipline in the domain of colloids and surfaces. The unusual optical properties of small gold particles, their size-dependent electrochemistry, and their high chemical stability have made them the model system of choice for exploring a wide range of phenomena including self-assembly, biolabeling, catalysis, electron-transfer theories, phase transfer, DNA melting and assays, and crystal growth. This review focuses on gold nanoparticles, specifically those on the small end of the nanoparticle dimension scale. These nanoparticles (NPs) when stabilized or protected by a shell of thiolate ligands display good stability toward aggregation and other modes of decay, which enables attempts at isolating different NP sizes and the exploration of how NP properties depend on size (including quantization effects). NPs with fewer than 300 Au atoms can display distinct optical and electronic properties compared to the bulk metal. The thiolated NP stability further enables treating the ligand shell as a chemical platform that can be manipulated to exhibit desired reactivities, polyfunctionalization, and optical properties. The consequence for the past couple of decades has been a very active field of basic nanoscience research and applications of these NPs. An important aspect of Au NPs has been the breadth of their impact; applications range from photonic device fabrications, to sensing of organic and biomolecules, to charge storage systems. The subject is too large for a comprehensive treatment in the space available, and we have accordingly made selections of areas to

highlight, with apologies to those omitted. Several complementary reviews on nanoparticles have appeared.<sup>1</sup>

A noteworthy recent observation has been that the ligation chemistry of very small thiolate-protected Au nanoparticles is not simply a head-on thiolate bonding to a consolidated Au core of atoms—a “standard model” assumption<sup>1</sup> of Au NP structure. X-ray crystallographic determinations<sup>2a-c</sup> of Au<sub>102</sub> and Au<sub>25</sub> nanoparticle structures show instead that the ligands are bonded in *bridging* coordination and many of the Au atoms are not part of the core but exist with the ligands in semiring or “staple” structures (Figure 1). The extent to which this structural motif extends to the thiolate interfaces of larger Au NPs remains to be seen. The success of DFT calculations<sup>2d</sup> in reproducing experimental semiring structural facts has put such calculations more firmly into play in understanding this topic.

The above structural discoveries followed detailed investigations of small thiolate-protected Au nanoparticles that had delineated spectroscopic and kinetic properties. The results of those investigations are now open to deeper interpretations in light of the Figure 1 structure. For example, the common procedure of replacing one Au surface ligand with another (ligand or place exchange)<sup>1</sup> must in view of Figure 1 involve a more complex, multiple bond-breaking pathway.

**Synthesis of Thiolate-Protected Au Nanoparticles.** The synthesis of small, monodisperse nanoparticles is a major challenge in nanotechnology research. Smaller particles experience increased driving forces to aggregate to diminish surface energy, so a protective coating, or “capping”, is necessary during synthesis to keep them in a finely dispersed state. Of the two distinct

<sup>†</sup> Part of the “Langmuir 25th Year: Nanoparticles synthesis, properties, and assemblies” special issue.

\*Corresponding authors. E-mail: mulvaney@unimelb.edu.au, rwm@email.unc.edu.

(1) (a) Templeton, A. C.; Wuelfing, W. P.; Murray, R. W. *Acc. Chem. Res.* **2000**, *33*, 27–36. (b) Daniel, M. C.; Astruc, D. *Chem. Rev.* **2004**, *104*, 293–346. (c) Murray, R. W. *Chem. Rev.* **2008**, *108*, 2688–2720. (d) Zabet-Khosousi, A.; Dhirani, A. *Chem. Rev.* **2008**, *108*, 4072–4124.

(2) (a) Jadzinsky, P. D.; Calero, G.; Ackerson, C. J.; Bushnell, D. A.; Kornberg, R. D. *Science* **2007**, *318*, 430. (b) Heaven, M. W.; Dass, A.; White, P. S.; Holt, K. M.; Murray, R. W. *J. Am. Chem. Soc.* **2008**, *130*, 3754–3755. (c) Zhu, M.; Aikens, C. M.; Hollander, F. J.; Schatz, G. C.; Jin, R. J. *Am. Chem. Soc.* **2008**, *130*, 5883–5885. (d) Akola, J.; Walter, M.; Whetten, R. L.; Hakkinen, H.; Gronbeck, H. *J. Am. Chem. Soc.* **2008**, *130*, 3756–3757. (e) Parker, J. F.; Choi, J.-P.; Wang, W.; Murray, R. W. *J. Phys. Chem. C* **2008**, *112*, 13976–13981.

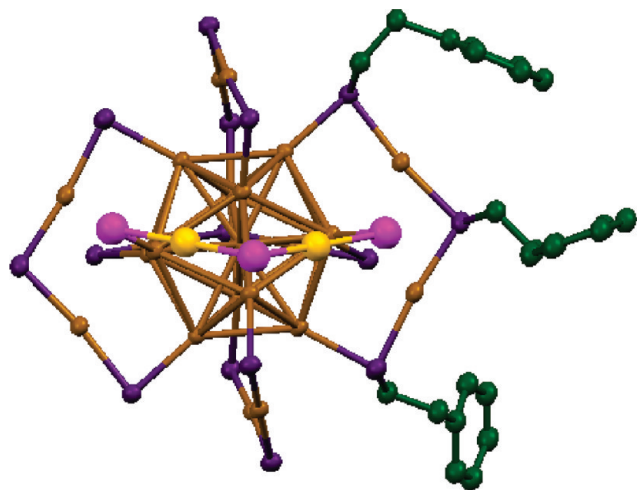


**Figure 1.** Simplified X-ray crystal structure of  $[\text{Oct}_4\text{N}^+][\text{Au}_{25}(\text{SC}_2\text{Ph})_{18}]^-$  adapted from ref 2e. Phenylethylene R groups (shown only for one semiring) have two different bridging thiolate coordinations. The  $-\text{SR}-\text{Au}-\text{SR}-\text{Au}-\text{SR}-$  semirings in the reduced MPC do not align in a plane, exhibiting a puckering of the semiring that is highlighted by brighter coloring. (Au = yellow, S = violet, C = green, and H not shown). Reprinted with permission from ref 2e. Copyright 2008 American Chemical Society.

strategies for making metal nanoparticles, (1) the top-down approach and (2) the bottom-up technique, the latter is by far the more common and effective. Metal ions are reduced by a reducing reagent; they nucleate to form nanoparticles while in the presence of protective ligands. Either the stoichiometry of the available metal ion supply or the passivation of further growth by the protective ligands can determine the eventual nanoparticle size.

A seminal early nanoparticle synthesis<sup>3a</sup> was of  $\text{Au}_{55}(\text{Ph}_3\text{P})\text{Cl}$ , whereby the complex  $[\text{Au}(\text{Ph}_3\text{P})\text{Cl}]$  was reduced with diborane gas. This nanoparticle proved to be difficult to isolate in a pure state and was somewhat unstable. A very influential<sup>3b</sup> subsequent synthesis protocol is outlined in Scheme 1, where following phase transfer of a gold salt into an organic medium—using a phase-transfer agent such as tetraoctylammonium bromide—and the addition of an organic thiol, an excess of a strong reducing agent—such as sodium borohydride—is added, with the rapid production of thiolate-protected Au nanoparticles. The parameters of the “B Brust synthesis” have been thoroughly explored.<sup>3c</sup> A major advantage is rough control over the average size of the synthesized particles by the choice of the reduction condition and the gold salt-to-thiol molar ratio used, but even then, in general postsynthesis size fractionation is necessary.

**Synthesis of Au Nanoparticles within Dendrimers.** Various dendrimer molecules have also been used to stabilize metal nanoparticles (including Au). Pioneering work by Crooks and co-workers<sup>4a</sup> substantially defined the nanoparticle stability inside the dendritic network and its further utilization (Figure 2). The advantages of the dendrimer approach include the following: (1) The completeness of reduction of the metal ions sequestered inside the dendrimer yields some stoichiometric control over the

nanoparticle size. The dendrimer arms are very effective at preventing nanoparticle aggregation. (2) The loose steric aspects of dendrimers also allow the encapsulated nanoparticles to participate in various catalytic reactions. (3) The terminal groups on the dendrimer periphery can be modified for purposes of nanoparticle solubility in different media, among other goals.

The encapsulation of metal ions inside dendrimers involves, variously, electrostatic and complexation interactions; the dendrimer interior includes coordinating groups such as  $-\text{OH}$ ,  $\text{NH}_2$ , or  $-\text{COOH}$ . Stable monodisperse Au NPs can be synthesized using quaternary ammonium-terminated fourth- and sixth-generation dendrimers without further purification steps. Water-soluble  $\text{Au}_8$  nanodots have also been prepared within hydroxy-terminated second- and fourth-generation ( $\text{G2-OH}$  and  $\text{G4-OH}$ ) dendrimers,<sup>4b</sup> and they fluoresce at short wavelengths that change with the size of the Au nanoparticle. In contrast, thiolated Au nanoparticles do not emit at shorter wavelengths but instead emit at relatively size-independent near-infrared wavelengths.

**Making Networks and Films of Thiolate-Protected Au Nanoparticles.** The formation of mono- and multilayer films of small-ligand-stabilized metal nanoparticles is a significant research topic given the variety of possible applications (separations, chemical sensors) and their significance in fundamental science (such as the ligand dependence of electron hopping conductivity within the films). The formation of gold colloid monolayers was reported in *Langmuir* in 1993 using electrophoretic deposition,<sup>5</sup> and the sophistication of the approaches has grown rapidly. Techniques<sup>1c</sup> employed to form multilayers include (1) ligand exchanges combined with dithiol linkers, (2) electrostatic or coordinative interactions with groupings present on the nanoparticle surface, (3) covalent linking using amide coupling, and (4) the LB method. A particularly straightforward method is coordinative coupling between carboxylate or sulfonate groups on the nanoparticle ligand shell with metal ions (such as  $\text{Cu}^{2+}$  or  $\text{Zn}^{2+}$ ). Multilayer films can be prepared in simple two-step dip and rinse cycles as illustrated in Figure 3.<sup>6a</sup> Polyelectrolytes such as cationic poly(allylamine hydrochloride) can also be used; in this case, the nanoparticle is itself effectively a polyelectrolyte imitating the layer-by-layer (LBL) technique.<sup>6b–6d</sup> By choice of the organic polyelectrolyte charge complement, this procedure is effective at building multilayers whether the nanoparticle ligand shell is cationic or anionic.

**Multimer Assemblies of Au Nanoparticles.** Multimers of nanoparticles are interesting chemical objects. A seemingly general approach to preparing them, say by ligand exchanges on the nanoparticle producing linker connections, encounters the challenge of controlling the number of such exchanges, with its underlying statistics. A sample containing an average of three exchanged ligands will actually contain a distribution of exchanged ligands, and excessive exchanges will yield nanoparticle aggregates. A solid-phase approach<sup>7</sup> can limit the number of linker ligand exchange sites by providing them with large (in comparison) polystyrene beads as illustrated in Figure 4. In the first step, a single acid-terminated thiolate is incorporated onto a 2 nm butanethiolate-protected nanoparticle; that entity is then released from the bead, and the resulting singly functionalized nanoparticle can become linked into dimers by amide coupling with aliphatic diamines. This method produced

(3) (a) Schmid, G.; Pfeil, F.; Boese, R.; Bandermann, F.; Meyer, S.; Calis, G. H. M.; van der Velden, J. W. A. *Chem. Ber.* **1981**, *114*, 3634. (b) Brust, M.; Walker, M.; Bethell, D.; Schiffrin, D. J.; Whyman, R. J. *Chem. Soc., Chem. Commun.* **1994**, 801–802. (c) Hostetler, M. J.; Wingate, J. E.; Zhong, C.-J.; Harris, J. E.; Vachet, R. W.; Clark, M. R.; Londono, J. D.; Green, S. J.; Stokes, J. J.; Wignall, G. D.; Gilsh, G. L.; Porter, M. D.; Evans, N. D.; Murray, R. W. *Langmuir* **1998**, *14*, 17–30.

(4) (a) Scott, R. W. J.; Wilson, O. M.; Crooks, R. M. J. *Phys. Chem. B* **2005**, *109*, 692–704. (b) Zheng, J.; Petty, J. T.; Dickson, R. M. J. *Am. Chem. Soc.* **2003**, *125*, 7780–7781.

(5) Giersig, M.; Mulvaney, P. *Langmuir* **1993**, *9*, 3408.

(6) (a) Zamborini, F. P.; Hicks, J. F.; Murray, R. W. *J. Am. Chem. Soc.* **2000**, *122*, 4514–4515. (b) Hicks, J. F.; Seok-Shon, Y.; Murray, R. W. *Langmuir* **2002**, *18*, 2288–2294. (c) Yu, A.; Liang, Z.; Cho, J.; Caruso, F. *Nano Lett.* **2003**, *3*, 1203–1207. (d) Decher, G. *Science* **1997**, *277*, 1232–1237.

(7) Worden, J. G.; Shaffer, A. W.; Huo, Q. *Chem. Commun.* **2004**, 518–519.

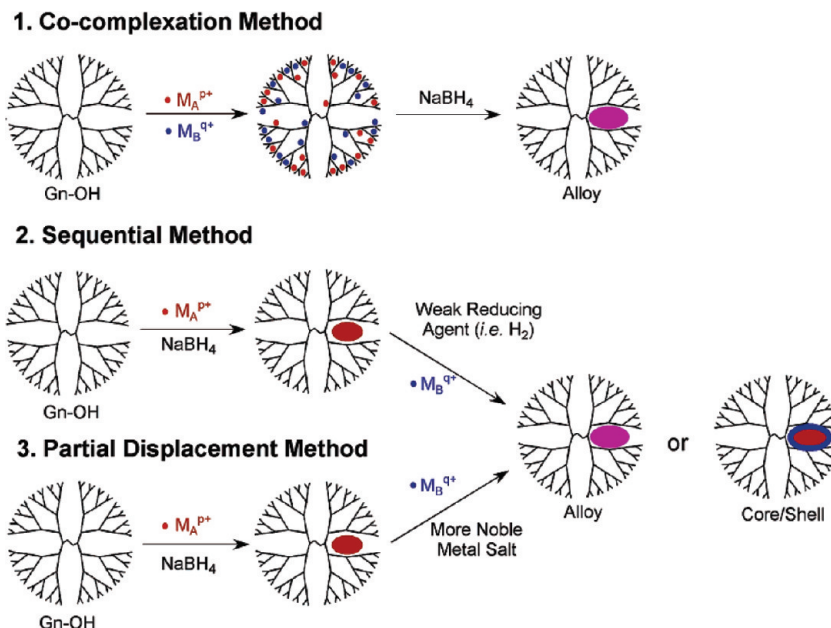
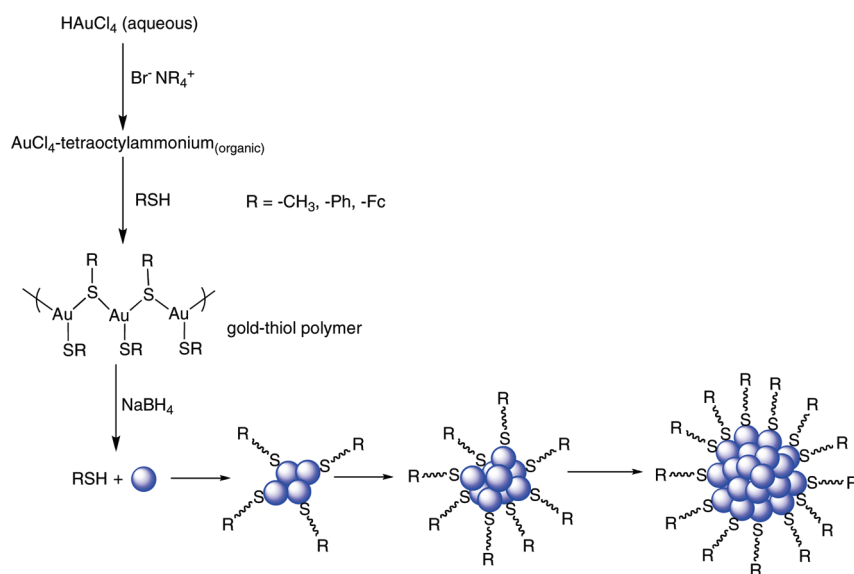


**Figure 2.** Cartoon depicting the synthesis of various metal nanoparticles using dendrimers as capping ligands. Reprinted with permission from ref 4a. Copyright 2005 American Chemical Society.

**Scheme 1. Scheme for Gold Nanoparticle Synthesis by the Brust Two-Phase Approach**



nanoparticles where 60–70% were dimers, along with some single particles and trimers.

In another nanostructure assembly creation, Stellacci and co-workers<sup>8</sup> prepared nanoparticles with mixed monolayers of functional ligands such as nonanethiolate and 4-methylbenzenethiolate. The disparities between these functional ligands caused a form of striped surface ordering, as in Figure 5A,B. Subsequent ligand exchange reactions (with 11-mercaptopundecanoic acid, MUA), according to the “hairy ball theorem”, were directed to the “poles” of the nanoparticles. Coupling of the MUA acid groups with a diamine (1,6-diaminohexane) leads to the formation of 1D nanoparticle chains. The interparticle distance inside the chain could be controlled by using different diamines such as *O,O'*-bis(2 aminoethyl)octadecaethylene glycol (EGDA).

**Gold as a Catalytic Nanoparticle.** Although gold nanoparticles have been used for many different purposes, their catalytic properties were for decades considered to be weak or absent. It was an exciting discovery then when Haruta and Hutchings simultaneously and independently<sup>9a,9b</sup> showed that gold could be very active, in particular, for the heterogeneous low-temperature oxidation of CO. It was found that bare gold nanoparticles were not active but when on a metal oxide support, such as  $\alpha$ -Fe<sub>2</sub>O<sub>3</sub>, became excellent catalysts for the oxidation of CO. It was first considered that the high activity resulted from a new type of composite oxide catalyst, but after a detailed electron microscopy study, it was found that the most active catalysts were small gold nanoparticles approximately 2–4 nm in diameter. The catalytically active nanoparticles form a reconstructed structure with the

(8) DeVries, G. A.; Brunnbauer, M.; Hu, Y.; Jackson, A. M.; Long, B.; Neltner, B. T.; Uzun, O.; Wunsch, B. H.; Stellacci, F. *Science* **2007**, *315*, 358–361.

(9) (a) Sanchez, R. M. T.; Ueda, A.; Tanaka, K.; Haruta, M. *J. Catal.* **1997**, *168*, 125–127. (b) Hashmi, A. S. K.; Hutchings, G. J. *Angew. Chem., Int. Ed.* **2006**, *45*, 7896–7936. (c) Thomas, K. G.; Kamat, P. V. *Acc. Chem. Res.* **2003**, *36*, 888–898.



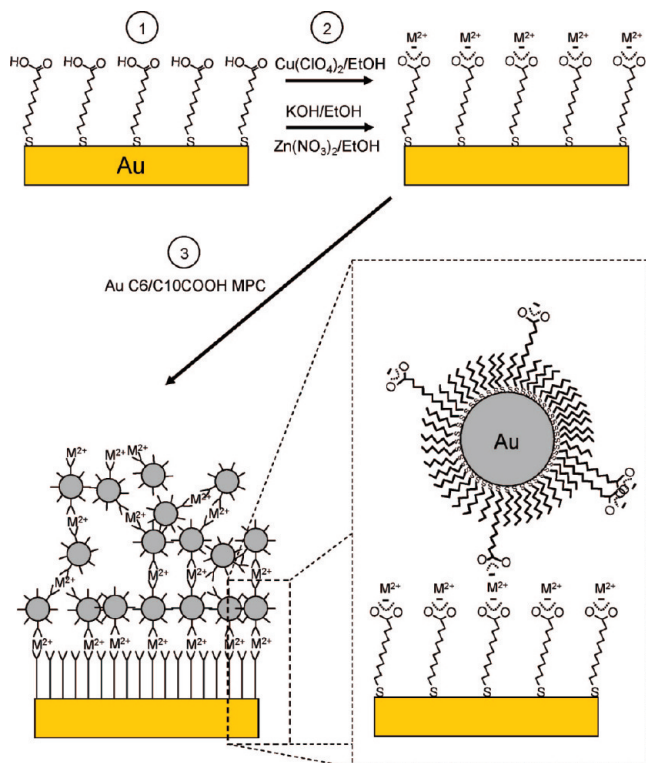


**Figure 3.** Scheme for forming multilayer films from mixed-monolayer Au nanoparticles. Adapted from ref 6c. Reprinted with permission from ref 1c. Copyright 2008 American Chemical Society.

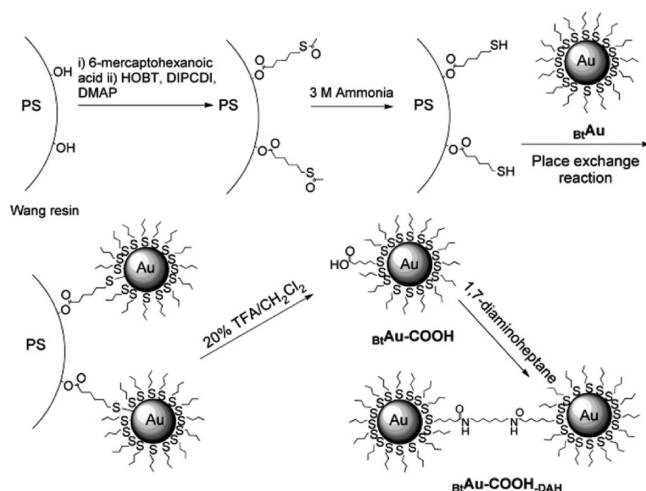


**Figure 4.** Synthetic outline of gold-nanoparticle dimer synthesis. Reprinted with permission from ref 7. Copyright 2004 The Royal Society of Chemistry.

substrate, and CO adsorption would proceed on the adjacent metal oxide. The reaction is thought to involve carbonate-like intermediates decomposing to  $\text{CO}_2$  upon desorption from the surface. This catalytic discovery spurred a substantial body of other studies on heterogeneous gold catalysis, including the hydrogenation of alkenes or alkynes, hydrosilylation, oxidation of alcohols, and photocatalysis.<sup>9c</sup> Au nanoparticles chemically attached to glassy carbon electrodes have also been used for the oxidation of CO and  $\text{CH}_3\text{OH}$  resulting in the formation of  $\text{CO}_2$ .<sup>1b</sup>

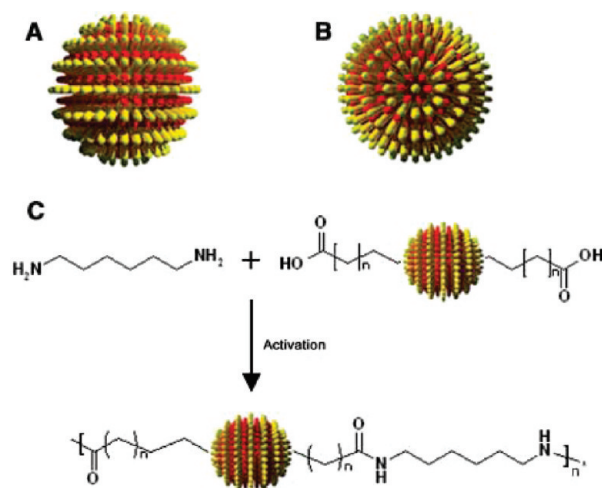


**Figure 5.** Synthetic approach of 1D nanoparticle chain formation. Reprinted with permission from ref 8. Copyright 2007 American Association for the Advancement of Science.

### Electrochemical Reactivities of Au Nanoparticles

Three categories of electrochemical behavior of solutions of thiolate-protected Au nanoparticles have been delineated. These categories cross the so-called metal-to-molecule transition region of nanoparticle size, and their voltammograms are labeled<sup>1c</sup> bulk-continuum voltammetry, quantized double-layer charging voltammetry, and molecule-like voltammetry. The observed voltammetric currents in all three are controlled by mass transport rates; they differ in the potential dependence of the currents (just as is the case for small redox molecules).

Another form of nanoparticle voltammetry involves cases where the protecting ligand shell is itself electroactive. The redox-labeled voltammetric reactions add to those underlying the nanoparticle itself. Another form of electroactivity is that of a strongly held, redox-active conjugate with the nanoparticle ligand shell, which has been used in various forms of DNA sensing in particular.

**Bulk-Continuum Voltammetry.** Just as ionic space charges—the electrical double layer—exist at all electrified metal/electrolyte solution interfaces, nanoparticles in solutions (colloids, metal sols, regardless of the metal, and semiconductor nanoparticles) have double layers with ionic surface excesses on the solution side that reflect any net electronic charge residing on the metal nanoparticle surface (or its capping ligand shell). In this light, one can say that all metal-like nanoparticles are intrinsically electroactive and act as electron donor/acceptors to the quantitative extent of their double-layer capacitances. The electron charge storage capacity, per nanoparticle, depends on the nanoparticle size (surface area), nanoparticle double-layer capacitance  $C_{\text{DL}}$ , and potential (relative to nanoparticle zero charge). This capacity can be quite substantial; for example, a 10-nm-diameter nanoparticle with  $C_{\text{DL}} = 120 \text{ aF}$  (equivalent to  $40 \mu\text{F}/\text{cm}^2$ ) can store  $\sim 750 \text{ e/V}$ . This capacity is capable, as a “colloidal micro-electrode”, of driving electrochemical reactions such as proton reduction to  $\text{H}_2$ . The quantitative demonstrations of this property by Henglein et al.<sup>10a</sup> and Gratzel et al.,<sup>10b</sup> starting in 1979, represented the beginning of the modern understanding of the electrochemistry of metal nanoparticles.

In the earliest experiments, nanoparticles were charged by chemical reactions. The transition to electrochemical control by

(10) (a) Henglein, A. *J. Phys. Chem.* **1979**, *83*, 2209. (b) Kiwi, J.; Gratzel, M. *J. Am. Chem. Soc.* **1979**, *101*, 7214.

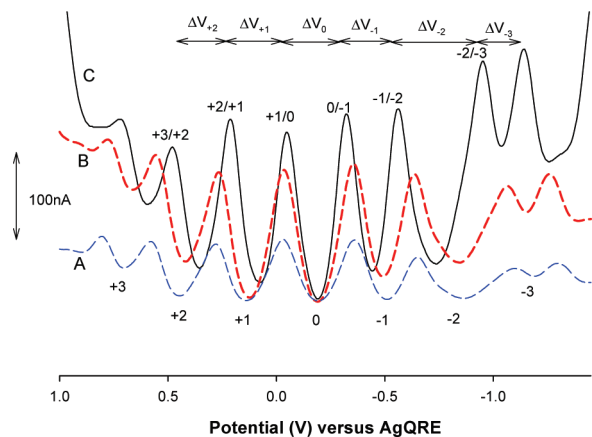


**Figure 6.** Osteryoung square-wave voltammetry (OSWV) of 0.08 mM  $\text{Au}_{1.40}(\text{SC6})_{53}$  (estimated monodispersity  $\sim 43\%$ , SC6 = hexanethiolate) in  $\text{CH}_2\text{Cl}_2$  at 283 K with  $\text{Bu}_4\text{NClO}_4$  concentrations of (A) 0.74 mM, (B) 1.02 mM, and (C) 100 mM. The voltammograms have been adjusted to a common  $E_{\text{PZC}}$  potential vs AgQRE (Ag wire quasireference electrode);  $E_{\text{PZC}}$  is about  $-0.2$  V with respect to Ag/AgCl. Reprinted with permission from ref 12b. Copyright 2005 American Chemical Society.

Ung et al.<sup>11</sup> was made by showing that solutions of Ag nanoparticles capped with poly(acrylic acid) could also be charged at (macroscopic) working electrodes, diffusing to undergo electron transfer at electrode/electrolyte interfaces. Although the observed current–potential curves (at potentials insufficiently positive to oxidize Ag) were featureless, the currents exceeded background values and varied with  $[\text{time}]^{-1/2}$  (in potential step experiments) and with  $[\text{rotation rate}]^{1/2}$  (in rotated disk electrode experiments)—characteristics of current control by diffusing entities according to the well-known Cottrell and Levich equations, respectively,

$$I(t) = \frac{nFAD_{\text{NP}}^{1/2}C_{\text{NP}}^{\text{BULK}}}{\pi^{1/2}t^{1/2}} \quad \text{and} \quad I_{\text{lim}} = 0.62nFAD_{\text{NP}}^{2/3}\omega^{1/2}\nu^{-1/6}C_{\text{NP}}^{\text{BULK}} \quad (1)$$

where  $D_{\text{NP}}$  and  $C_{\text{NP}}^{\text{BULK}}$  are the Ag nanoparticle diffusion coefficient and concentration. Thus, even though a metal nanoparticle yields no voltammetric wave and exhibits no discrete “formal potential”, its electrochemical charging is observable and demonstrable by the application of mass transport criteria.

**Quantized Double-Layer Charging (QDL).** The metal-like nanoparticle’s double layer can become quantized if its size and consequently capacitance  $C_{\text{DL}}$  are much smaller, for the same reasons that coulomb staircase charging is observed in solvent-free experiments on solid-state nanostructures. QDL solution voltammetry was in fact compared to scanning tunnelling spectroscopy data in the initial experimental observations. Better-defined features were observed (Figure 6) in subsequent experiments<sup>12</sup> owing mainly to improved purification of the nanoparticle studied.

Observing discretized double-layer charging as in Figure 6 depends on the equation<sup>1c</sup>

$$\Delta V = e/C_{\text{DL}} \quad (2)$$

where  $e$  is the electron charge and  $\Delta V$  is the nanoparticle potential change incurred upon a *single* electron transfer to/from a working electrode or any other electron donor/acceptor.  $\Delta V$  is the voltage spacing between the waves in Figure 6. These nanoparticles are “quantum capacitors”, with their stored-charge potentials changing by palpable values upon single electron transfers.

The essential requirement to observe QDL voltammetry is a sufficiently small value of  $C_{\text{DL}}$  (e.g., a very small nanoparticle and a low dielectric ligand shell). These features are expressed in the concentric sphere capacitor model that was introduced to approximate the nanoparticle capacitance  $C_{\text{DL}}$

$$C_{\text{DL}} = A_{\text{NP}} \frac{\epsilon\epsilon_0 r + d}{r} = 4\pi\epsilon\epsilon_0 \frac{r}{d}(r + d) \quad (3)$$

where  $A_{\text{NP}}$ ,  $r$ , and  $r + d$  are the nanoparticle surface area, radius, and radius plus protecting ligand layer thickness (of effective dielectric constant  $\epsilon$ ). This model asserts that the QDL wave spacing  $\Delta V$  should be inversely proportional to the effective dielectric constant of the capping shell. Importantly, if  $\Delta V$  is  $< \sim k_{\text{B}}T$  (25.7 meV at 25 °C)—the Boltzmann distribution of thermal energy—then the QDL waves are smeared together, single-electron-transfer behavior is obscured, and nanoparticle double-layer charging falls into the bulk-continuum voltammetric regime. This should occur for  $C_{\text{NP}} \approx 6$  aF per nanoparticle. Equally importantly, if the nanoparticle sample is a mixture of sizes small enough to display QDL voltammetry, then the overlap of differently spaced QDL patterns will obscure all except possibly those features closest to  $E_{\text{PZC}}$  (as shown by simulations).

Early studies of QDL showed that  $\Delta V$  values for alkanethiolate-coated Au nanoparticles scale with chain length<sup>1c</sup> as predicted by eq 3 (within ca. 10% in most cases) and at low electrolyte concentration display a maximum at the nanoparticle potential of zero charge ( $\Delta V_0$  in Figure 6), as anticipated for a radially dispersed *diffuse* double layer.<sup>12b</sup> Equation 3 is most obviously an approximation in the variable “ $\epsilon$ ” when solvent and/or electrolyte ions permeate the ligand shell, as has been reported. Theoretical efforts have been aimed at improvements to the concentric sphere capacitor model.<sup>1c</sup> QDL behavior is also severely distorted when alkanethiolate-coated Au nanoparticles are placed (as a film on the working electrode) in an aqueous medium in which they are decidedly not soluble. Finally, eq 3 and other theories must now be considered in light of the revised structural picture of the Au/thiolate nanoparticle surface (Figure 1).

**Molecule-Like Voltammetry.** The progression of properties from large to smaller nanoparticles—continuum voltammetry to QDL voltammetry—culminates in the emergence of molecularity in the smallest nanoparticles, as signaled by the presence of HOMO–LUMO gaps and by structure in nanoparticle electronic spectra. This metal-to-molecule transition is seen in changes in optical band edge energies and by the interruption of the regular spacing of QDL voltammetric patterns by a central larger spacing.<sup>13</sup> As Figure 7A illustrates,<sup>14</sup> the potential of the first reduction step, in this case of the nanoparticle  $\text{Au}_{25}\text{L}_{18}^-$ , is substantially separated (1.6 V) from that of its first oxidation step ( $\text{Au}_{25}\text{L}_{18}^{0/-}$  couple). The 1.6 V separation is the HOMO–LUMO gap energy plus a charging energy term that can be estimated using the 0.3 V (electrostatic) spacing of the doublet of waves between 0 and +0.5 V. This gives a 1.3 V HOMO–LUMO energy estimate which is in accordance with an optical

(11) Ung, T.; Giersig, M.; Dunstan, D.; Mulvaney, P. *Langmuir* **1997**, *13*, 1773.

(12) (a) Ingram, R. S.; Hostetler, M. J.; Murray, R. W.; Schaaf, T. G.; Khoury, J.; Whetten, R. L.; Bigioni, T. P.; Guthrie, D. K.; First, P. N. *J. Am. Chem. Soc.* **1997**, *119*, 9279. (b) Guo, R.; Georganopolou, D.; Feldberg, S. W.; Donkers, R.; Murray, R. W. *Anal. Chem.* **2005**, *77*, 2662.

(13) Chen, S.; Ingram, R. S.; Hostetler, M. J.; Pietron, J. J.; Murray, R. W.; Schaaff, T. G.; Khoury, J. T.; Alvarez, M. M.; Whetten, R. L. *Science* **1998**, *280*, 2098.

(14) Lee, D.; Donkers, R. L.; Wang, G.-L.; Harper, A. S.; Murray, R. W. *J. Am. Chem. Soc.* **2004**, *126*, 6193.

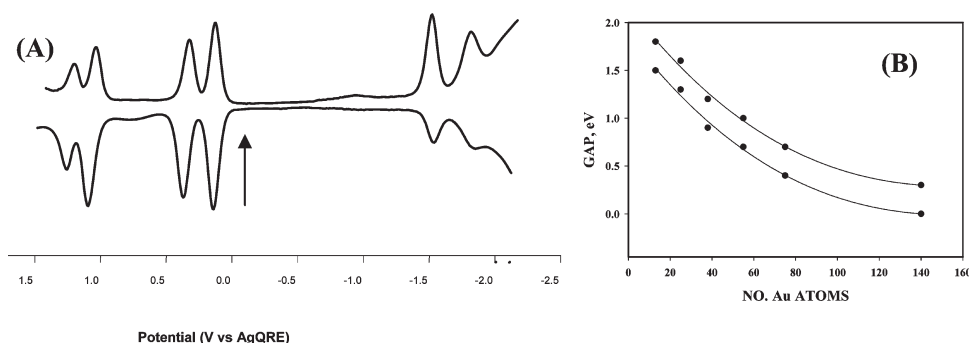


**Figure 7.** (A)  $-70^{\circ}\text{C}$  differential pulse voltammogram (DPV, sampled current vs  $E$ ) at  $0.02\text{ V/s}$  for  $\text{Au}_{25}(\text{PhC}_2\text{S})_{18}$  in  $0.1\text{ M Bu}_4\text{NPF}_6$  in degassed  $\text{CH}_2\text{Cl}_2$  at a  $0.4\text{-mm}$ -diameter Pt working, Ag wire quasireference (AgQRE), and Pt wire counter electrode. The arrow indicates the solution rest potential. (The original report misidentified this nanoparticle as  $\text{Au}_{38}\text{L}_{24}$ .) Adapted from ref 14. (B) Plot of electrochemical energy gaps (upper curve) and estimated HOMO–LUMO energy gaps (subtract  $0.3\text{ eV}$ ) against the estimated number of Au atoms in thiolate-protected nanoparticles. Reprinted with permission from ref 1c. Copyright 2008 American Chemical Society.

band edge measurement. The doublet of waves is another molecule-like aspect of the voltammogram in Figure 7A; such doublets are common in molecular electrochemistry for electrode reactions of a doubly occupied molecular orbital.

The HOMO–LUMO and electrochemical gap energies are sensitive to the nanoparticle size, as illustrated by Figure 7B. This diagram captures a central goal of research for small Au nanoparticles, and we hope that in time it will be supplemented by further more exacting atom counts for the isolated Au nanoparticle fractions and by theoretical analyses. The experimental  $\text{Au}_{25}\text{L}_{18}^-$  HOMO–LUMO gap of  $1.3\text{ V}$  has been verified.<sup>2d</sup>

**Redox-Labeled Nanoparticle Voltammetry.** Attaching electroactive thiolates to Au nanoparticles was explored early in the development of the Au nanoparticle field. Thus, a Brust reaction preparation (Scheme 1) using a mixture of  $\omega$ -ferrocene-hexanethiols and hexanethiols produced mixed-monolayer Au nanoparticles with 10–15 ferrocenes/nanoparticle.<sup>15</sup> Their voltammetry is a combination of the expected ferrocene oxidation wave and the double-layer charging of the Au core; each is identifiable by the choice of potential region and an analysis of nanoparticle mass transport behavior. Interestingly, the ferrocene wave shape displayed the characteristics of a single-electron redox process (i.e.,  $n = 1$  in a Nernstian analysis) in which the effective concentration of ferrocene sites is simply larger by 10–15-fold (i.e., the multiple redox sites undergo very rapid, serial electron-transfer reactions as identical noninteracting sites). This is the same behavior as demonstrated much earlier for redox polymers such as polyvinylferrocene,<sup>15,16</sup> illustrating an analogy between classical functionalized polymers and functionalized nanoparticles. The thermodynamic aspects of electron transfer should of course not especially depend on the geometrical shape of the object to which the redox sites are affixed.

The kinetic aspects of multiple electron transfers of redox groups on nanoparticles are interesting in light of the question, how can all of the multiple redox groups coating the Au nanoparticle undergo reaction during a single diffusive encounter (of duration  $\tau_{\text{ENCOUNTER}} \approx d^2/D_{\text{NP}}$ ) with an electrode surface? Three reaction pathways<sup>15b</sup> for redox sites can be identified: (A) reaction through the nanoparticle core by electron tunneling through twice the thickness  $2(d-r)$  of the protective ligand layer

at a rate ( $\text{s}^{-1}$ ) of  $\sim k_{\text{ET}}^{\circ} \exp[-2\beta(d-r)]$  where  $k_{\text{ET}}^{\circ}$  is the self-exchange rate constant for a contact encounter; (B) lateral site–site electron hopping over the nanoparticle circumference at a rate of  $k_{\text{HOP}} = D_{\text{E,2D}}/2\pi^2 r^2$  where  $D_{\text{E,2D}}$  is the 2D electron diffusion coefficient (which depends on  $k_{\text{ET}}^{\circ}$ , the surface spacing of the redox groups, and the flexibility of the structures linking them to the nanoparticle surface); and (C) rotational diffusion, where nanoparticle rotation brings each redox site into the proximity of the electrode for electron transfer at a rate of  $k_{\text{ROT}} = 3k_{\text{B}}T/4\pi r^3\eta$  where  $\eta$  is the solution viscosity. The rates of these pathways—one of which must exceed  $\tau_{\text{ENCOUNTER}}$  for complete reaction—show that process C is more likely for smaller nanoparticles ( $r$ ) whereas process A becomes more likely for a thinner ( $d-r$ ) or more electron-transmissive (smaller  $\beta$ ) linking structure. The deliberate design of the electron-transfer pathway should be possible.

A further analogy between classical functionalized polymers and functionalized nanoparticles lies in their polyelectrolyte properties. Polyelectrolytes are well known for their propensity to adsorb on oppositely charged surfaces (e.g., the layer-by-layer process of polyanion layer buildup).<sup>6d</sup> The strong adsorption is reinforced by the charge site–site multiplicity, which is akin to the well-known metal complex chelate effect and is based, at least in part, entropically on the partial liberation of the solvation shell of the site–site partners. This effect seems to extend to multiply charged nanoparticles and was first discovered by the strong adsorption of polyferrocenated Au NPs and is now extended to nearly irreversible adsorptions on various electrodes of nanoparticles bearing ligand shells terminated by polyquaternary ammonium functions.<sup>17</sup>

### Nanoparticle Ligand Exchange and Modification Reactions

Nanoparticles are capped or protected by shells of ligands; an added value is an ability to alter the chemistry of the shell. This has been done by (a) exchanging the protecting ligand with a different protecting and desirably functionalized ligand (ligand or “place” exchange) or (b) by reactions on a functionalized protecting ligand, such as forming an amide bond with a  $-\text{CO}_2\text{H}$  function to an amine reagent.<sup>1a</sup> Often, method a is followed by method b.

(15) Green, S. J.; Stokes, J. J.; Hostetler, M. J.; Pietron, J. J.; Murray, R. W. *J. Phys. Chem. B* **1997**, *101*, 2663–2668. (b) Green, S. J.; Pietron, J. J.; Stokes, J. J.; Hostetler, M. J.; Vu, H.; Wuefing, W. P.; Murray, R. W. *Langmuir* **1998**, *14*, 5612–5619.

(16) Flanagan, J. B.; Margel, S.; Bard, A. J.; Anson, F. C. *J. Am. Chem. Soc.* **1978**, *100*, 4248–4253.

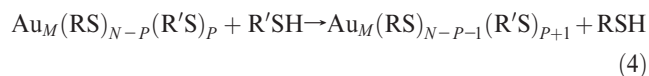
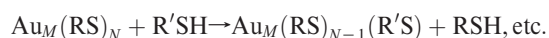
(17) (a) Stiles, R. L.; Balasubramanian, B.; Feldberg, S. W.; Murray, R. W. *J. Am. Chem. Soc.* **2008**, *130*, 1856–1865. (b) Sardar, R.; Beasley, C. A.; Murray, R. W. *Anal. Chem.* Submitted for publication. (c) Sardar, R.; Beasley, C. A.; Murray, R. W. Unpublished results, UNC-CH.



Two different ligand exchanges have been extensively employed for Au nanoparticles. One is the exchange of the weakly attached citrate ligand—for Au nanoparticles prepared by the classical citrate reduction route—with an organic thiol or a mixture of thiols. This is a relatively simple procedure in which one can reasonably assume that the exchange reaction proceeds to exhaustion. Its introduction to the modification of Au nanoparticles with thiolated ssDNA structures and the elaboration of nanoparticle assemblies by the binding of complementary ssDNA strands was an important addition to nanoparticle chemistry.<sup>18</sup> Mirkin showed how the introduction of an oligonucleotide duplex with ends complementary to mixtures of nanoparticles bearing sequences complementary to the duplex (but noncomplementary to each other) could cause nanoparticle aggregation (plus color and spectral changes). The aggregation could be reversed by thermally “melting” (denaturing) the complements. The high specificity of this scheme and the many ways in which it could be elaborated to become more sensitive to analytically detect specific ssDNA analyte strands have led to a robust research area of bioanalytical chemistry.<sup>19</sup>

The exchange of thiolate ligands on nanoparticles prepared by the Brust reaction<sup>1a,1b</sup> with other thiolate ligands, or mixtures thereof, is a more reluctant reaction, owing to the strength of Au–SR binding, but can be accomplished and has also become widely exploited. In the context of preparing and subsequently purifying (and core size selecting) thiolate-protected nanoparticles, one soon recognizes that their solubility and other (chromatographic, electrophoretic) properties are dominated by the ligand shell. Therefore, it becomes strategically advantageous to learn to prepare and size isolate with a convenient thiolate ligand and subsequently to change the ligands as desired using ligand exchange reactions. Exchanges of simple alkanethiolate ligands with  $\omega$ -functionalized thiols was a principal route to demonstrating an array of further nanoparticle functionalizations, such as those used in Figure 3 above.<sup>5a</sup>

The exchange of one thiolate ligand with another is a serial process:



NMR measurements show that the liberated RS– ligand appears as its thiol conjugate acid. If the exchange is random with respect to ligand location (i.e., binding sites have equal accessibility and reactivity and noninteractive with one another), then necessarily the number of exchanged ligands,  $P$ , on individual nanoparticles varies statistically as a Poisson distribution, as recently demonstrated.<sup>20</sup> Examining the obedience to such random statistics is a potential window to detecting differences in the binding chemistry of thiolate ligands across the nanoparticle surface (e.g., the “coordination chemistry” of the nanoparticle).

The kinetics of ligand exchange is another window on the binding chemistry of thiolate-protected Au nanoparticles. Studies have variously focused on kinetic behavior early<sup>21</sup> in an exchange

and on longer-time reactions that approach equilibrium.<sup>22</sup> The former follow second-order kinetics, and the latter have been fitted to Langmuir diffusion kinetics. While the exchange process is—like a ligand exchange of a metal complex—a seemingly elemental reaction, the discovery of semirings as discussed in connection with Figure 1 has introduced further complexity. For example, in the  $\text{Au}_{25}\text{L}_{18}$  structure, *two* RS–Au bonds must be broken and replaced with new R'S–Au bonds. Features of ligand behavior that have been interpreted in terms of nanoparticle core vertices and terraces have to be revisited in light of the added complexity of structural detail of the nanoparticle surface.

## Surface Plasmon Spectroscopy with Metal Nanoparticles

In the preceding, the different ways that cyclic voltammetry can be used to study electron-transfer reactions involving small gold nanocrystals was discussed. The particles can be dispersed in solution or adsorbed as films or may simply react with redox couples in solution. The fact that these crystals form optically clear, homogeneous solutions makes spectroscopic studies particularly attractive.

Surface plasmon spectroscopy (SPS) has been used to study small metal crystals for some 50 years, dating back at least to Doyle,<sup>23</sup> although the unusual colors of gold nanocrystals have been exploited for centuries. SPS is a versatile technique for studying chemisorption, redox reactions, (bio)sensing, alloying, and electrochemical processes such as underpotential deposition involving small metal nanocrystals that exhibit well-defined surface plasmon modes.<sup>24</sup> This includes Au, Ag, Cu, Sn, Pb, Hg, Cd, In, and the alkali metals. The keys to this broad range of applications are the equations governing surface plasmon excitation in metal particles. For particles much smaller than the wavelength of light, the emission and absorption of light are dominated by the dipolar plasmon mode, and the normalized cross sections for these are given by

$$Q_{\text{abs}} = 4\pi\text{Im} \left[ \frac{\epsilon - \epsilon_m}{\epsilon + \left(\frac{1-L}{L}\right)\epsilon_m} \right] \quad (5a)$$

$$Q_{\text{sca}} = \frac{8\pi^4}{3} \left| \frac{\epsilon - \epsilon_m}{\epsilon + \left(\frac{1-L}{L}\right)\epsilon_m} \right|^2 \quad (5b)$$

Here,  $x = 2\pi(\epsilon_m)^{1/2}(a/\lambda)$ ,  $\epsilon(\lambda) = \epsilon' + i\epsilon''$  is the wavelength-dependent dielectric function of the metal,  $\epsilon_m = n^2$  is the dielectric function of the surrounding medium, and  $L$  is the shape factor of the particle, which may be calculated numerically if the exact morphology is known. Color changes can occur as a consequence of changes in particle shape, which alter the shape factor  $L$ , whereas surface adsorption alters the refractive index  $\epsilon_n$  of the medium or region near the particle. Modified versions of these equations can be used for core–shell nanocrystals, and SPS was validated by monitoring silica shell growth on spherical gold nanocrystals in 1996 by Liz-Marzan et al.<sup>25</sup> The core–shell model is also necessary when modeling the optical properties of alkanethiolate-protected gold nanoparticles as discussed by

(18) (a) Mirkin, C. A.; Letsinger, R. L.; Mucic, R. C.; Storhoff, J. J. *Nature* **1996**, *382*, 607. (b) Alivisatos, A. P.; Johnsson, K. P.; Peng, X.; Wilson, T. E.; Loweth, C. J.; Bruchez, M. P., Jr.; Schultz, P. G. *Nature* **1996**, *382*, 609–612.

(19) Rosi, N. L.; Mirkin, C. A. *Chem. Rev.* **2005**, *105*, 1547.

(20) Dass, A.; Holt, K.; Parker, J. F.; Feldberg, S. W.; Murray, R. W. *J. Phys. Chem. C* **2008**, *112*, 20276–20283.

(21) (a) Guo, R.; Murray, R. W. *J. Am. Chem. Soc.* **2005**, *127*, 12140. (b) Guo, R.; Song, Y.; Wang, G.; Murray, R. W. *J. Am. Chem. Soc.* **2005**, *127*, 2752–2757.

(22) Kassam, A.; Bremner, G.; Clark, B.; Ulibarri, G.; Lennox, R. B. *J. Am. Chem. Soc.* **2006**, *128*, 3476–3477.

(23) Doyle, W. T. *Phys. Rev.* **1958**, *111*, 1067.

(24) Mulvaney, P. *Langmuir* **1996**, *12*, 788.

(25) Liz-Marzan, L. M.; Giersig, M.; Mulvaney, P. *Langmuir* **1996**, *12*, 4329.

Templeton et al.<sup>26</sup> The Drude model for the dielectric properties also includes the electron density in the metal. This means that changes in particle charge can be followed spectroscopically and SPS can be used to monitor electrochemical events. The surface plasmon resonance shift depends on the electron density according to eq 6.<sup>27</sup>

$$\Delta\lambda = -\frac{\Delta N}{2N}\lambda_p\sqrt{\epsilon_\infty + \left(\frac{1-L}{L}\right)\epsilon_m} \quad (6)$$

Here,  $N$  is the electron density in the uncharged gold nanorod,  $\epsilon_\infty$  is the high-frequency contribution to  $\epsilon'$ , and  $\lambda_p$  is the bulk plasma wavelength. Hence, if the electron density changes to  $N + \Delta N$ , then the bulk plasma wavelength changes correspondingly, along with the position of the surface plasmon peak. Electron transfer from electrodes to particles and from solution-phase species to reductants can consequently be observed;<sup>11</sup> in addition, Fermi-level equilibration between metal and semiconductor nanocrystals can be directly inferred through SPS.<sup>28</sup>

### Shape Effects of Metal Nanocrystals

One of the major reasons for the continuing importance of SPS in studying metal nanocrystals has been the explosion of interest in the shape-controlled synthesis of metal particles. Although there had been reports of rodlike gold particles being produced in surfactants, the use of CTAB during the electrochemical reduction of gold salts to produce gold rods reported by Wang and colleagues in 1997 initiated a flurry of activity.<sup>29</sup> Over the last 10 years, it has become possible to control the morphology or crystal habit of small metal nanocrystals systematically, with pioneering studies by Xia and colleagues,<sup>30</sup> the Liz-Marzan group,<sup>31</sup> and Pileni and co-workers, among others.<sup>32</sup> Shape control is most often achieved via a two-step process known as “seed-mediated growth”. In the first step, small seed particles of gold are generated under conditions of high chemical supersaturation leading to a fast nucleation rate and therefore uniform, spherical nuclei of 1–5 nm. These conditions ensure the rapid growth of all crystal surfaces but are contraindicated for shape control. In the second step, a growth step, the reaction conditions are altered, more gold ions and a different reductant are added, together with some form of shape-templating surfactant or molecule, and the seeds are grown into larger particles with predetermined morphology. Typically, the growth stage is much slower and proceeds under milder reducing conditions than the nucleation stage. Common crystal morphologies that can be produced in high yield include rods, octahedra, decahedra, trigonal prisms, trigonal plates, hexagonal plates, and nanostars. Despite these advances, many colloidal preparations contain a large percentage of other shapes. A key issue remains the critical role of the seeds used to grow different types of nanocrystals.<sup>33</sup> Crystals grown in this way

are generally larger than the gold spheres discussed earlier and are the topic of the following discussion.

As can be seen from eq 5a, shape changes to a crystal alter the surface plasmon energies through changes to the parameter  $L$ . The values of  $L$  are predicted through numerical solutions using approaches such as DDA, FDTD, and BEM.<sup>34</sup>  $L$  changes with both the size and shape of the crystals and is strongly influenced by surface defects, roughness, and the quality of facets. By monitoring absorption spectra, the growth and changes in the morphology of crystals can be monitored in real time.<sup>35</sup>

Why the gold surface can be so selectively passivated is also unclear. In the case of gold rods, both rod growth and rod dissolution are spatioselective, occurring preferentially at the tips.<sup>36</sup> The high curvature implies that at a steady-state redox potential the electric field intensity will be higher. This so-called “lightning rod effect”<sup>37</sup> can dominate redox reactions and leads to facet-dependent growth and dissolution kinetics. Despite the tremendous progress in the synthesis of gold nanocrystals with different morphologies including rods, prisms, cubes, right pyramids, decahedra, octahedra, dodecahedra, and more complex structures such as dumbbells, there is as yet little work on the electrochemistry of such particles.

### Single-Nanoparticle Experiments

The need to investigate the optical properties of metal particles of a single, well-defined shape and size has motivated the development of a number of new techniques. Arrays of relatively monodisperse nanosized disks or triangles may be fabricated using electron-beam lithography (EBL) or nanosphere lithography.<sup>38–40</sup> These techniques rely on metal evaporation through a mask and result in polycrystalline particles. The cumulative signal from the array of particles allows their investigation via optical transmission spectroscopy. Another approach has been laser-based absorption techniques for the interrogation of single metal particles.<sup>41</sup> These techniques allow for the investigation of the vibrational dynamics of single particles;<sup>42</sup> however, the complexity of the equipment required for these experiments has not led to their widespread use. In contrast, following pioneering work by Feldmann et al. to determine the far-field spectra of individual gold nanoparticles via elastic scattering,<sup>43</sup> a number of new techniques based upon the scattering of light by metal particles have been developed. Perhaps the most common of these is dark-field microscopy (DFM) in which the particles are excited using either an evanescent field from totally internally reflected light or a dark-field condenser with a central beam block to form a hollow cone of light. A schematic diagram of a dark-field condenser along with a dark-field image of gold nanorods is shown in Figure 8a. It should be noted that in this

(26) Templeton, A. C.; Pietron, J. J.; Murray, R. W.; Mulvaney, P. *J. Phys. Chem. B* **2000**, *104*, 564.

(27) Mulvaney, P.; Perez-Juste, J.; Giersig, M.; Liz-Marzan, L. M.; Pecharroman, C. *Plasmonics* **2006**, *1*, 61.

(28) Wood, A.; Giersig, M.; Mulvaney, P. *J. Phys. Chem. B* **2001**, *105*, 8810.

(29) Yu, Y. Y.; Chang, S. S.; Lee, C. L.; Wang, C. R. C. *J. Phys. Chem. B* **1997**, *101*, 6661–6664.

(30) Xia, Y.; Lim, B.; Jiong, Y.; Skrabalak, S. E. *Angew. Chem., Int. Ed.* **2009**, *48*, 60.

(31) Liz-Marzan, L. M. *Langmuir* **2006**, *22*, 32.

(32) Pileni, M.-P.; Ninham, B. W.; Gulik-Krzywicki, T.; Tanori, J.; Lisiecki, I.; Filankembo, A. *Adv. Mater.* **1999**, *11*, 1358.

(33) Grzelczak, M.; Jorge Pérez-Juste, J.; Mulvaney, P.; Liz-Marzán, L. M. *Chem. Soc. Rev.* **2008**, *37*, 1783–1791.

(34) Myroshnychenko, V.; Rodriguez-Fernandez, J.; Pastoriza-Santos, I.; Funston, A. M.; Novo, C.; Mulvaney, P.; Liz-Marzan, L. M.; de Abajo, F. J. G. *Chem. Soc. Rev.* **2008**, *37*, 1792.

(35) Perez-Juste, J.; Pastoriza-Santos, I.; Liz-Marzan, L. M.; Mulvaney, P. *Coord. Chem. Rev.* **2005**, *249*, 1870.

(36) Rodriguez-Fernandez, J.; Perez-Juste, J.; Mulvaney, P.; Liz-Marzan, L. M. *J. Phys. Chem. B* **2005**, *109*, 14257.

(37) Burda, C.; Chen, X.; Narayanan, R.; El-Sayed, M. A. *Chem. Rev.* **2005**, *105*, 1025–1102.

(38) Chan, G. H.; Zhao, J.; Hicks, E. M.; Schatz, G. C.; van Duyne, R. P. *Nano Lett.* **2007**, *7*, 1947.

(39) Sonnichsen, C.; Geier, S.; Hecker, N. E.; von Plessen, G.; Feldmann, J.; Dittbacher, H.; Lamprecht, B.; Krenn, J. R.; Aussenegg, F. R.; Chan, V. Z. H.; Spatz, J. P.; Moller, M. *Appl. Phys. Lett.* **2000**, *77*, 2949.

(40) Gwinner, M. C.; Koroknay, E.; Fu, L. W.; Patoka, P.; Kandulski, W.; Giersig, M.; Giessen, H. *Small* **2009**, *5*, 400.

(41) Boyer, D.; Tamarat, P.; Maali, A.; Lounis, B.; Orrit, M. *Science* **2002**, *297*, 1160.

(42) Staleva, H.; Hartland, G. V. *Adv. Funct. Mater.* **2008**, *18*, 3809.

(43) Klar, T.; Perner, M.; Grosse, S.; Plessen, G. v.; Spirkel, W.; Feldmann, J. *Phys. Rev. Lett.* **1998**, *80*, 4249.



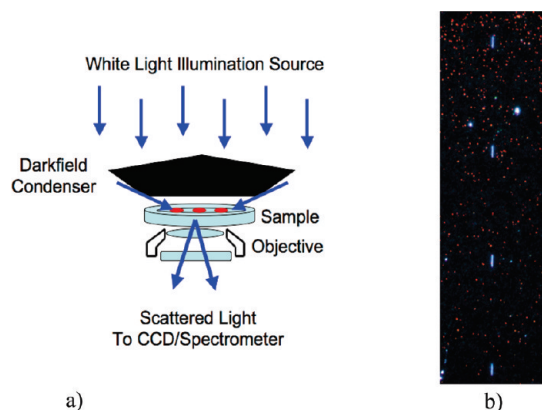


**Figure 8.** (a) Schematic diagram of the dark-field experiment. (b) Dark-field image of gold nanorods (red spots) dispersed on an ITO-coated glass slide. The white marks are etches in the substrate made using the focused ion beam (FIB), and the edges of the etches scatter white light.

experimental setup, surface plasmon modes with a dipole moment in the plane of the substrate dominate the scattering. The Rayleigh scattering is size- and shape-dependent and scales as the sixth power of the particle diameter (for a sphere); this places a lower practical limit on the size of particles that can be detected of 40–50 nm. Absorption techniques are able to measure the optical properties of particles as small as 2.5 nm.<sup>41</sup>

Although it is an elegant technique, SPS of single particles introduces its own challenges. For example, it is not possible to unambiguously determine the size and shape of the actual particle giving rise to a particular scattering spectrum. To circumvent this issue, a routine, reliable method for using electron microscopy and DFM on the same nanocrystals using a focused ion beam to etch markers on the substrate has recently been developed (Figure 8b).<sup>44</sup> Another problem is that the particles are dispersed on a glass substrate, often in a polymer film, so the environment is no longer homogeneous. This means that  $\epsilon_m$  in eq 5b is no longer well-defined. The substrate effect can be estimated in the electrostatic limit using the method of images. The effective refractive index of particles dispersed in varying amounts of the polymer polyvinylalcohol (PVA) and on various substrates has been determined experimentally using single-particle spectroscopy.<sup>45</sup>

### Selected Emerging Areas

**Electron Transfer on Single Particles.** Electron-transfer studies have generally been restricted to measurements of ensemble-averaged rate constants, masking the important role of the shape and size of nanocrystals. This has profound implications for the fundamental reactions involving water splitting to form hydrogen and also the oxidation of pollutants such as CO. A major challenge is therefore to understand the relationship between the nanocrystal structure and the rates of electron exchange with redox couples and hence to design and synthesize optimized catalysts for these reactions. One step in this direction for very small Au nanoparticles has been the recent discovery of a structure-change-induced component of the self-exchange electron transfer in the couple  $\text{Au}_{25}\text{L}_{18}^{0/-}$ . Is this effect dependent on the thiolate ligand L?

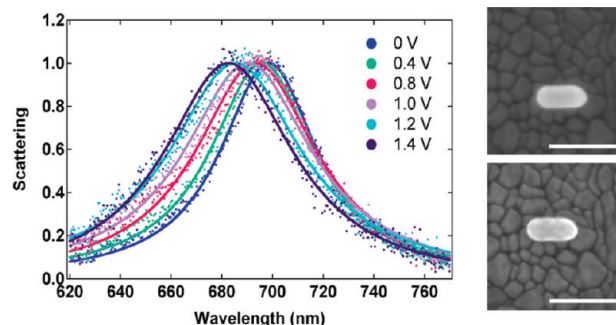


**Figure 9.** Normalized scattering spectra of the gold nanorod shown in the SEMs at right (top image taken before charging, bottom image taken after charging) at different potentials varying from 0 to  $-1.4$  V. The solid lines are Lorentzian fits to the spectra. The granular structure visible in the micrographs is from the ITO surface. Scale bars = 100 nm.

Another important step was the recent report of the direct observation of redox reactions on single nanocrystals.<sup>46,47</sup> An electron transfer rate of 4600 e/s was directly measured during the gold-catalyzed oxidation of ascorbic acid by dissolved oxygen in a catalytic cycle monitored via surface plasmon spectroscopy.<sup>46</sup> The electrons could also be injected electrochemically and their surface plasmon band could be monitored in situ in a specially designed electrochemical cell using an optically transparent indium tin oxide (ITO) substrate (Figure 9). This experiment is reminiscent of the OTTLE cell developed in the 1960s for spectro-electrochemistry. Cyclical shifts of the particle plasmon resonances were observed at negative biases and correlation of the surface plasmon spectra of the particles with their morphology determined that the plasmon shifts were largest for nanorods.<sup>44</sup>

The excess electrons present within a nanoparticle following chemical injection by ascorbic acid can also be used to reduce  $\text{AuCl}_4^-$  to gold metal in the presence of cetyltrimethylammonium bromide (CTAB). Using this scheme, the growth of a single gold nanorod was observed in real time. In this case, the lowest-energy surface is at the tip of the rod, and the deposition of even a small amount of gold will result in a relatively large red shift in the nanocrystal spectrum because of the change in the aspect ratio (and hence  $L$  in eq 1). The observed increase in the aspect ratio measured corresponded to the deposition of 100 atoms of gold every second.<sup>47</sup>

The sensitivity of the above measurements is limited by the intrinsic SP band shift per electron added and by the signal-to-noise collection efficiency of the CCD spectrometer. Improved signal-to-noise ratios, for example, by detecting changes around the surface plasmon resonance using lock-in techniques, open up the intriguing possibility of studying the “quantum reaction” regime involving single-molecule transfer or electron transfer at nanocrystal surfaces.

**Mechanical Coupling.** SPS provides an unusual method for probing the mechanical properties of metal nanocrystals. The excitation of a small plasmon-active metal particle by a femtosecond laser pulse launches the fundamental vibrational modes of the particle. For rods, there are some 50 modes readily derived from finite element modeling, but two dominate, the breathing mode and stretching mode.<sup>48</sup> Other modes are observed in cubes and core-shell particles. These studies lead to the direct

(44) Novo, C.; Funston, A. M.; Pastoriza-Santos, I.; Liz-Marzán, L. L.; Mulvaney, P. *Angew. Chem., Int. Ed.* **2007**, *46*, 3517.

(45) Novo, C.; Funston, A. M.; Pastoriza-Santos, I.; Liz-Marzán, L. M.; Mulvaney, P. *J. Phys. Chem. C* **2008**, *112*, 3.

(46) Novo, C.; Funston, A. M.; Gooding, A. K.; Mulvaney, P. Submitted for publication, 2008.

(47) Novo, C.; Funston, A. M.; Mulvaney, P. *Nat. Nanotechnol.* **2008**, *3*, 598.

(48) Hu, M.; Wang, X.; Hartland, G. V.; Mulvaney, P.; Juste, J. P.; Sader, J. E. *J. Am. Chem. Soc.* **2003**, *125*, 14925.

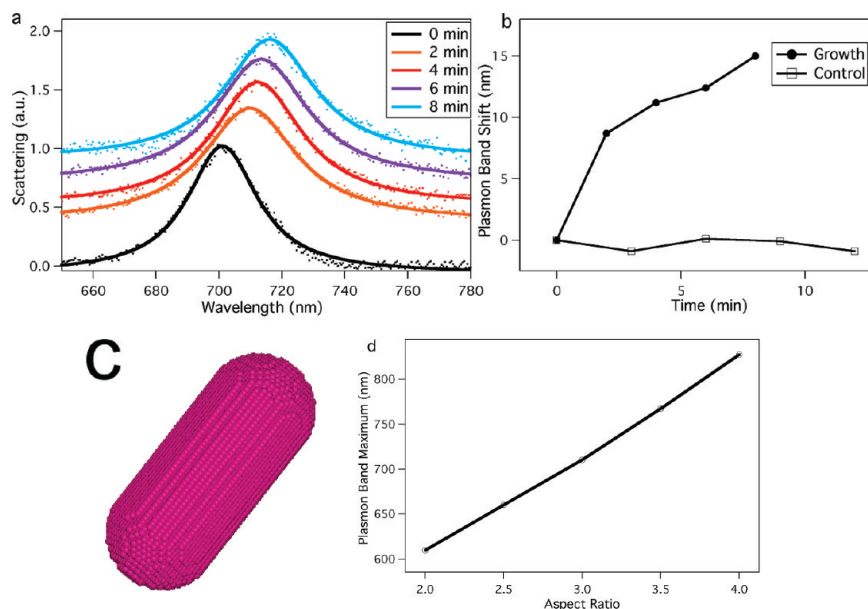


**Figure 10.** Growth of a single gold nanorod. (a) Evolution of the scattering spectrum of a gold nanorod (aspect ratio 2.87) after a growth solution containing CTAB,  $\text{HAuCl}_4$ , and ascorbic acid (reducing agent) is added. The spectra are normalized, and the solid lines are the Lorentzian fits to the experimental data. (b) SP band position as a function of time for the growth experiment and for a control experiment. The error bars represent the error in determining the peak position from the Lorentzian fitting procedure. (c) Typical DDA target constructed to simulate hemispherically capped gold nanorods containing 52 000 dipoles and an aspect ratio of 2.87. (d) Predicted SP position versus aspect ratio for hemispherically capped rods in a medium with relative permittivity  $\epsilon_m = 2.025$  based on DDA results. Reprinted with permission from ref 47. Copyright 2008 Nature Publishing Group.

measurement of the Young's modulus of the metal. For gold, a weakening of the bulk modulus is observed. This is due to the decrease in the coordination number of the surface atoms, which dominates the increased surface stress. These measurements also allow the rate of heat transfer into the medium to be obtained. This intense, local heating effect is exploited in photothermal cancer therapy, in which cells labeled with metal nanocrystals are destroyed using laser irradiation.

**Plasmonics.** A direct consequence of the localized surface plasmon resonances of metal nanoparticles is an enhancement of the field close to the nanoparticle surface, known as the near field. The close approach (i.e., within 2.5 times the particle diameter) of two nanoparticles leads to the interaction of their localized surface plasmon resonances. The coupling of the plasmon resonances of metallic nanoparticles has recently emerged as a strategic area widely applicable across physics, chemistry, and biology. The driving force behind these potential applications is the formation of highly enhanced, localized electromagnetic fields in the coupled structures. The "hot spots" created by localized electromagnetic fields from the nanoparticles allow the detection of single molecules via surface-enhanced Raman spectroscopy (SERS).<sup>49</sup>

Surface plasmons propagate along the surface of metals, providing a means to confine, guide, and focus energy using subwavelength structures such as EBL-fabricated nanometer thin metal strips or nanostructured surfaces. It has recently been found that chemically synthesized gold and silver nanowires are also able to act as waveguides for visible light.<sup>50</sup> This phenomenon is echoed by interacting single particles where the coupling of nanoparticles spaced less than two diameters apart results in the transmission of light energy down a nanoparticle chain.<sup>51</sup>

The near-field interaction between nanoparticles is highly distance-dependent and has been described using an electromagnetic analogue of molecular orbital theory, the plasmon hybridization model.<sup>52</sup> While the distance dependence has recently been approximated as an exponential function in the plasmon ruler equation and exploited for the measurement of distances within biological systems,<sup>53</sup> it is only recently that limits for the accuracy of the exponential function have been determined at small interparticle separations.<sup>54</sup>

Dimer formation leads to a lowering of the symmetry of the system with respect to the monomer. When the incoming electric field is oriented along the interparticle axis (for a given particle pair), the near fields couple in a manner analogous to a bonding interaction resulting in a red shift of the plasmon resonance.<sup>52,55</sup> When the polarization is oriented perpendicular to the interparticle axis, their near fields couple in a nonbonding type of interaction, and a very small blue shift of the plasmon band is observed.<sup>52</sup> For each of these arrangements, the other possible interaction mode is a dark mode that cannot be excited by light because of the symmetry of the system. When the initial nanoparticles are themselves nanorods rather than spherical, a large number of coupling geometries become possible between both longitudinal (along the length of the nanorod) and transverse (along the width of the rod) plasmon resonance modes. The coupling between each of these modes mirrors the features observed for coupling between spheres as shown in Figure 11 for the longitudinal mode. A further lowering of the symmetry leads to the generation of a number of coupling modes (Figure 11). These have recently been described in detail.<sup>54</sup>

(49) Nie, S.; Emory, S. R. *Science* **1997**, 275, 1102.

(50) Sanders, A. W.; Routenberg, D. A.; Wiley, B. J.; Xia, Y.; Dufresne, E. R.; Reed, M. A. *Nano Lett.* **2006**, 6, 1822.

(51) Maier, S. A.; Kik, P. G.; Atwater, H. A.; Meltzer, S.; Harel, E.; Koel, B. E.; Requicha, A. A. G. *Nat. Mater.* **2003**, 2, 229.

(52) Prodan, E.; Radloff, C.; Halas, N. J.; Nordlander, P. *Science* **2003**, 302, 419.

(53) Sönnichsen, C.; Reinhard, B. M.; Liphardt, J.; Alivisatos, A. P. *Nat. Biotechnol.* **2005**, 23, 741.

(54) Funston, A. M.; Novo, C.; Davis, T. J.; Mulvaney, P. *Nano Lett.* **2009**, 9, 1651.

(55) Sardar, R.; Heap, T. B.; Shumaker-Parry, J. S. *J. Am. Chem. Soc.* **2007**, 129, 5356–5357.

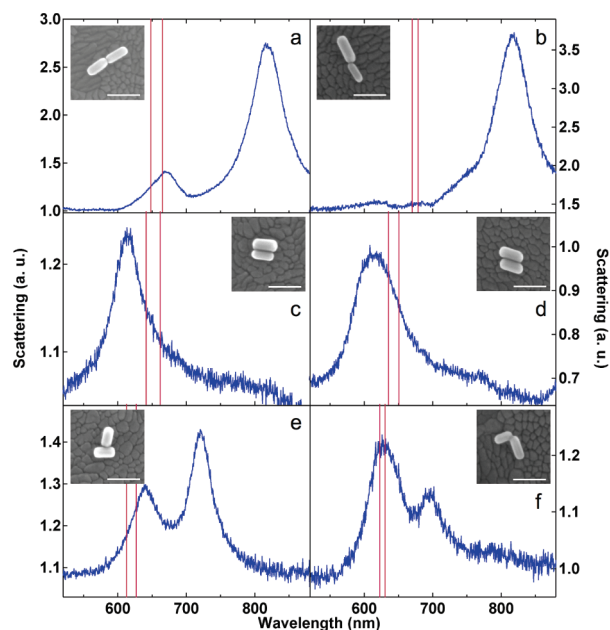


**Figure 11.** Scattering spectra of various gold rod dimers and (inset) electron micrographs of the same dimers showing the different configurations. Reprinted with permission from ref 54. Copyright 2009 American Chemical Society.

### Analytical Measurements of Nanoparticle Composition.

There is nothing quite like knowing the composition of a chemical that you are investigating—it lends scope and clarity to interpretations of chemical and physical behavior. In the nanoparticle arena, this is a challenging topic that can be imagined in steps: (a) What is the composition in terms of the element ratio? (b) What is its molecular mass? (c) What is its actual structure? Step a is easily accessible with modern analytical tools such as ICP-MS, at least as an average composition for incompletely size-fractionated nanoparticles. (One realizes that the ratio of surface ligands to nanoparticle core atoms is a function of size). Step c suffers and will continue to suffer from barriers to insufficient purification by nanoparticle core size (or ligand count). It can be expected that either purification methods will have to be improved enormously or synthetic procedures will have to be developed that intrinsically limit nanoparticle growth at some determined point. With respect to the latter point, perhaps the thinking of polymer chemists on catalysts that produce monodisperse polymer chains can be usefully adopted.

As for step b, the determination of molecular formula or mass, the most appealing approach but still a highly formidable one, is via mass spectrometry in which fragmentation occurs to a small enough extent that the parent nanoparticle ion can be registered. This problem is beginning to yield, at least at the smallest Au nanoparticle sizes. Tsukuda et al.<sup>56</sup> recently presented pioneering data identifying a nanoparticle formula as Au<sub>144</sub>L<sub>59</sub>. The mass spectral resolution even for this accomplishment is barely sufficient, and improvements must beckon. We believe that adopting the tactics of protein mass spectrometrists, wherein the focus is placed on higher charges so as to lower the  $m/z$  ratio, is an important route to enlarging the access to larger nanoparticle formulas and to inspecting the mass details of smaller ones more closely.

(56) Chaki, N. K.; Negishi, Y.; Tsunoyama, H.; Shichibu, Y.; Tsukuda, T. *J. Am. Chem. Soc.* **2008**, *130*, 8608–8610.

**Electron Transfer in Nanoparticle Assemblies.** In this perspective, we have discussed charging processes involving colloidal dispersions of gold nanocrystals and the charging of single nanocrystals. These data and model systems provide the starting point for the modeling of charge transport in gold assemblies. In principle, self-assembly techniques offer the possibility to engineer macroscopic gold structures that have tunable electronic properties. Conduction in such structures may be controlled by tunneling or hopping. This may represent the next big step for gold nanocrystal electronics. An excellent comprehensive review has recently been provided by Zabet-Khosousi et al.,<sup>1d</sup> and readers are referred there for details.

**More of the Future—Blue Sky.** The development of thiolate-protected gold clusters has enabled the electron-transfer regime between molecules and macroelectrodes to be explored for the first time. Likewise, SPS offers complementary information to  $I$ – $V$  data on the rates of electron transfer and equilibration involving metal nanocrystals. These and other objectives retain many challenges and give rise to the following suggestions for research directions:

- (1) Unlike molecules or quantized Au<sub>25</sub> or Au<sub>140</sub> clusters, the double-layer capacitance of a 10 nm metal nanocrystal is substantial enough that tens, hundreds, or even thousands of electrons must move between an electrode and a particle in order to equalize their Fermi levels. The mechanism, whether tunneling or dielectric breakdown (“nanosparking”), has not been established. The electric field between an electrode and a particle during closest approach exceeds 10<sup>9</sup> V/m, orders of magnitude above the dielectric strength of water.<sup>10</sup>
- (2) Au clusters provide boxes for storing free single electrons. The chemical and spin properties of these unpaired single electrons have not been studied. Only very recently<sup>57</sup> has the EPR of a nanoparticle known to contain an odd electron count been reported. It is interesting to speculate on whether redox reaction mechanisms and catalysis may be different when only one electron is available for transfer from an isolated odd-electron nanoparticle.
- (3) The preceding discussion provokes the thought that if the electronic coupling constant  $\beta$  were very small could the multiple electron-transfer reactions of the nanoparticle redox groupings become significant in chemical catalysis? This interesting thought has so far borne no fruit. However, that electronic coupling between redox sites attached to nanoparticles can be strong enough to effect light-promoted intervalent charge transfers between redox sites—as predicted by Hush four decades ago—was recently demonstrated.<sup>58</sup> This provocative observation suggests that continuing attention be paid to fashioning multielectron catalysts based on multifunctionalized redox nanoparticles.

### Summary

This is the 25th year of *Langmuir*, and the journal has been growing up at a time when the investigation of nanoscale

(57) Manzhou Zhu, M.; Aikens, C. M.; Hendrich, M. P.; Gupta, R.; Qian, H.; Schatz, G. C.; Jin, R. *J. Am. Chem. Soc.* **2009**, *131*, 2490–2492.

(58) Chen, W.; Chen, S.; Ding, F.; Wang, H.; Brown, L. E.; Konopelski, J. P. *J. Am. Chem. Soc.* **2008**, *130*, 12156.



phenomena has dominated many domains of science. Therefore, it is perhaps not surprising that quantized electron transport and nanoparticles have played a prominent role in many *Langmuir* papers in the journal thus far. However, it should also be noted that gold nanocrystals are aesthetically pleasing, chemically noble, and environmentally benign. A better model

system for understanding the world of colloids and surfaces is yet to be found.

**Acknowledgment.** The preparation of this article was supported in part by grants from the Office of Naval Research and the National Science Foundation (R.W.M.).